2017 International Conference on
Unmanned Aircraft Systems (ICUAS)
June 13-16, 2017, Miami, FL, USA

Proof of concept of micro-UAV-based radar imaging

Giancarmine Fasano, *Member, IEEE*, Alfredo Renga, Amedeo Rodi Vetrella, *Student Member, IEEE*, Giovanni Ludeno, Ilaria Catapano, and Francesco Soldovieri

***Abstract*— The potential of micro-UAV-based radar imaging is far from being exploited, though radar sensors having budgets compatible with micro-UAV are increasingly available. As a contribution to this topic, this paper discusses the relation between UAV dynamics and navigation, and radar processing, and presents a proof-of-concept ground imaging experiment in which a commercial hexacopter has been equipped with an ultralight radar. Flight results are presented in terms of both raw data and images obtained by means of an ad-hoc data processing approach. Results suggest that, in spite of its accuracy limitations, standalone GNSS information can be effectively integrated within radar processing algorithms, thus improving ground target detection and localization performance.**

I. Introduction

In recent years, Unmanned Aircraft Systems (UAS) have proven their value in a wide range of applications. Miniaturization of flight control systems and payloads also contributed to an increasing diffusion of micro-Unmanned Aerial Vehicles (UAVs), both in fixed wing and rotary wing configurations [1].

Micro-UAS can be a powerful tool in several fields, and well assessed applications exist which are typically based on optical cameras (daylight or infrared) and/or active LIDARs. Indeed, typical surveillance, surveying, and 2D/3D mapping missions are based on these sensors [2,3].

In this frame, radar systems can significantly improve micro UAS remote sensing capabilities, paving the way for the new applications and missions. In fact, they are capable of performing missions in all-weather and day/night conditions and, thanks to the ability of microwaves to penetrate materials, they allow detection and localization not only of surface objects but also of subsurface/hidden targets.

However, micro-UAV-borne radar imaging represents still a new frontier. Indeed, although airplane or helicopter mounted radars have been considered for surface and subsurface surveys and tomographic approaches have been proposed to image hidden targets [4], at present, radars onboard UAVs are mainly limited to medium/large platforms with significant mass, size, power and cost budgets.

G. Fasano, A. Renga, and A.R. Vetrella are with the Department of Industrial Engineering, University of Naples "Federico II", P.le Tecchio 80, 80125 Napoli, Italy (e-mails: giancarmine.fasano@unina.it, alfredo.renga@unina.it, amedeorodi.vetrella@unina.it).

G. Ludeno, I. Catapano, and F. Soldovieri, are with the Institute for Electromagnetic Sensing of the Environment (IREA) - National Research Council of Italy (CNR) Napoli, Italy (e-mails: ludeno.g@irea.cnr.it, catapano.i@irea.cnr.it, soldovieri.f@irea.cnr.it).

The basic reason is that implementation of micro-UAV-based radar poses a number of challenges at both system and processing level. First of all, besides above mentioned budgets, integration challenges also comprise processing and storage requirements, which may be hard to fulfill given the limited resources typically available onboard small unmanned aircraft. Then, since extraction of useful information is based on multi-temporal processing, key issues involve synchronization of navigation and radar data, navigation accuracy with respect to observation requirements related to the radar wavelength, and perturbed micro UAV dynamics in outdoor environments.

Thus, Micro-UAV radar imaging is, indeed, much more than a matter of technology miniaturization or payload installation, and it entails scientific challenges in terms of electromagnetic modeling and flight dynamics knowledge and control. For instance, ad-hoc and sophisticated data processing approaches are demanded to compensate for the limited performance of small, lightweight platforms and acquisition systems. Therefore, despite Synthetic Aperture Radar (SAR) imaging is a well assessed remote sensing tool, its adaption to micro-UAV is an open issue and few examples concerning the integration of SAR and micro UAV technologies have been reported world-wide [5]. In addition, only very preliminary results concerning subsurface imaging via UAV mounted radar have been provided [6].

Within this framework, this paper presents a proof-of-concept experiment conceived to investigate the above reported issues and verify ground imaging capabilities of an existing ultralight radar embarked on a commercial hexacopter. Specifically, radar and navigation data have been acquired, synchronized, and processed by adopting tomographic techniques developed for ground penetrating radar applications. The work results from the collaboration between the Department of Industrial Engineering (DII) of the University of Naples "Federico II" (UNINA) and the Institute for Electromagnetic Sensing of the Environment (IREA) - National Research Council of Italy (CNR).

Its main contributions can be summarized as follows:

- it discusses navigation requirements and algorithms for tomographic reconstruction;

- it describes hardware/software integration of the radar sensor on board the considered micro UAV;

- it shows an example of ground object detection and localization based on the assembled experimental setup.

It is worth noting that while this paper deals with radar imaging, different and important applications of radar sensor

onboard micro-UAV can be envisaged, including radar odometry for navigation and sense and avoid. The interested reader is referred to [7] for further details.

The paper is organized as follows. Section II deals with navigation challenges related to radar operation, while Section III discusses the adopted radar imaging approach. After a brief description of the experimental setup (Section IV), the paper finally reports results from low altitude flight experiments with on surface located corner reflectors.

II. Micro-UAV Navigation and Radar

Several examples are available of compact radar systems, whose mass, size, power and cost budgets are compatible with installation on micro-UAV [7]. However, in addition to radar data processing approaches that are discussed in the next section, flight dynamics of micro-UAV poses some challenges towards radar operation.

Classic assumption of straight path with constant speed is never verified even if short time span are considered. Radar imaging can be enabled for irregular platform motion provided that accurate reconstruction of platform trajectory can be performed. The required accuracy of the reconstructed trajectory depends on the considered imaging approach. However, a standard need sets the accuracy to be a fraction of radar wavelength, that is from less than 1 mm to a few cm depending on the working frequency band of the adopted radar system.

From the point of view of the flying platform, the possibility to estimate the trajectory with high-accuracy relies on the quality of the embarked navigation sensors, most notable ones including inertial measurement units (IMU) and Global Navigation Satellite Systems (GNSS) receivers. The achievable position and velocity accuracy is strongly dependant on the available GNSS measurements. Focusing the attention on GPS (though the discussion is general to all satellite navigation systems), differential GPS techniques, e.g. Carrier-phase Differential GPS (CDGPS) and Real-time Kinematic (RTK), represent a relatively mature solution to achieve cm-scale trajectory accuracy [8]. However, besides considering that this performance can be unsatisfactory for high-frequency W- and K-band radars, it is also worth noting that dual-frequency GPS receivers required to apply standard RKT algorithms involves the use of high-precision GPS antennas and high technology GPS receivers thus leading to mass, size and cost budgets which may prevent installation on micro-UAV. RTK approaches can also be followed with single frequency receivers, paying the cost of longer convergence times and reduced performance in terms of availability and integrity of the solution. In addition, RTK and differential GPS techniques can fail [9] under typical micro-UAS dynamics, which tend to be neither mild nor gentle.

Consequently, standalone GPS still remains a candidate for trajectory reconstruction. This can be implemented by integrated receiver and very compact lightweight patch antennas. The drawback of standalone GPS is the achieved positioning accuracy. The standalone GPS accuracy specifications provided by the US Department of Defense [10] are given assuming 1.5 m User Equivalent Range Error (1σ) and considering 2.3 and 4.4 Horizontal Dilution of Precision (HDOP) and Vertical Dilution of Precision, as typical mean value, respectively. This leads to several meters horizontal errors and about 10 m vertical errors, thus making the use of standalone GPS for radar imaging by micro-UAS of very limited practical usefulness.

Nonetheless, a more careful analysis of both GPS error sources and trajectory reconstruction requirements suggests that proper usage of GPS raw measurements can allow improved accuracy to be achieved. Specifically, the above-discussed standalone GPS performance is referred to absolute positioning accuracy, that is position estimates performed in a global reference frame, such as WGS84. On the contrary in radar imaging applications, the absolute location of the sensor, and so of the UAV too, is of limited relevance and the introduced trajectory requirements are actually referred to the relative trajectory of the UAV with respected to the observed scene. This is a crucial consideration to understand how trajectory reconstruction can be performed with much better accuracy than standalone GPS specifications. Specifically, standalone GPS accuracy specifications classify the error sources into two main categories [11]: system error sources including broadcast clock, broadcast ephemeris and group delay and user error sources such as ionospheric delay, tropospheric delay, multipath and receiver noise. Excluding the last two error sources, all the other ones are strongly correlated both in space and time [11]. Because of this correlation they introduce a position error that can be interpreted as an almost constant bias. In addition to this bias, and considering multipath-free environments, the position error shows a random-like behavior depending on receiver noise. Typical noise is in the order of 10-20 cm for pseudorange observables and less than 1 cm for carrier phase ones.

Based on this consideration, for reasonably short time intervals, relative (i.e., incremental) trajectory can be reconstructed by standalone GPS receiver with high-accuracy, up to a few cm. In detail, since the vast majority of GPS error sources are correlated, most of the positioning error is uniform in space and constant in time so it can be accommodated in the starting absolute location of the receiver. The knowledge of such a starting absolute location does not contribute to relative trajectory reconstruction whose accuracy is therefore determined by GPS measurement noise. In other words, even if the absolute location of the receiver cannot be determined with sufficient accuracy, the relevant estimate of receiver velocity is much more accurate [12] and can be used to define an accurate relative trajectory as done in odometry. Processing carrier-phase measurements, together with pseudorange ones, further reduces measurement noise and so relative trajectory errors.

III. Radar Imaging Algorithms

In general, radars are devices for detection and ranging of targets. An antenna transmits an electromagnetic wave (incident field E_{inc}) that, impinging on the targets, gives rise to a backscattered electromagnetic field (scattered field E_s).

This signal, which accounts for the target features, is gathered by a receiving antenna and processed to obtain a 2D image, providing information about the presence and location of target.

Radar imaging is a well assessed active electromagnetic tool for remote and in situ non-invasive surveys and it is exploited to generate high-resolution images (from centimetres to few meters) of the investigated region, which allow detection and localization of hidden targets, being microwave signals able to penetrate dielectric materials.

Generally speaking, time-domain radar imaging is performed by transmitting a modulated time domain pulse and by collecting the reflected energy as a function of time, which represents the travel-time of the wave along the transmitter-target-receiver path. By shifting the transmitting and receiving antennas along a line Γ at an altitude z far from the air-soil interface (see Figure 1) and joining together the gathered traces at all the antenna positions, a spatial-time image is built, which is referred to as raw-data "radargram" or B-scan. Being the round-trip travel time a function of the distance occurring between antennas and targets, the radargram provides a distorted image of the detected objects. These appear, indeed, as hyperbolas, whose characteristic features (i.e., vertex and eccentricity) depend on the object position, shape, size and electromagnetic properties of the probed medium [13].

Since a radargram is a codified representation of the scenario under test, its interpretability may strongly depend on the user expertise. Therefore, radar imaging usefulness, especially in complex environments, looks like limited.

To overcome this drawback, data processing approaches based on physical based models of the electromagnetic scattering are worth being considered, since they provide focused images, from which it is possible to infer an accurate characterization, in terms of geometrical parameters (i.e., location, size and shape), of the objects [14].

In the last years, the research activities of some of the authors have been focused on the development of microwave tomographic approaches able to deal with different scenarios and measurement configurations [15-18].

For these approaches, the targets are looked for as electromagnetic anomalies with respect to the background medium. The scattering phenomenon, which is at the basis of the sensing, is modelled according to the Born Approximation, which allows us to formulate the imaging as a linear inverse problem [19]. Therefore, the imaging is performed by using the truncated Singular Value Decomposition (SVD) as an effective regularized procedure capable of ensuing a stable solution of the linear inverse problem at hand[20].

By referring the reader to [16] for a detailed description of the imaging approach, in the following its mathematical formulation is summarized.

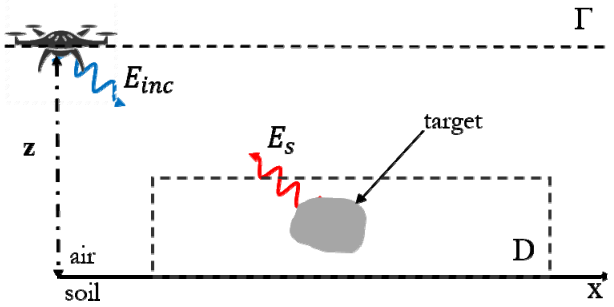

Figure 1. Reference scenario

Let $E_s(\mathbf{r}_m,\mathbf{r}_s\ \omega)$ be the scattered field measured at the generic point $\mathbf{r}_m$ and angular frequency ω when the transmitting antenna is at $\mathbf{r}_s$, and let $\chi(\mathbf{r})=(\varepsilon_x(\mathbf{r})/\varepsilon_b-1)$ be the unknown electric contrast function, $\varepsilon_x(\mathbf{r})$ being the unknown permittivity and ε_b the permittivity of the probed medium. Therefore, the relationship between the scattered field data and the unknown electric contrast function is described by the linear integral equation:

$$E_s(\mathbf{r}_m,\mathbf{r}_s,\omega)=k_b^2\int_D G(\mathbf{r}_m,\mathbf{r},\omega)E_{inc}(\mathbf{r},\mathbf{r}_s,\omega)\chi(\mathbf{r})d\mathbf{r} \tag{1}$$

where $k_b=\omega\sqrt{\varepsilon_b\mu_0}$ is the wave number in probed medium (air in the case at hand), while E_{inc} *and* G are the incident field and the Green's function, respectively. The points $\mathbf{r}_m$, $\mathbf{r}_s$ are on the measurement surface Γ and $\mathbf{r}$ is a generic point into the investigated domain D

After the discretization of the integral equation (1), the imaging is faced by solving the matrix inversion problem:

$$\mathbf{E}_s=\mathbf{L}\boldsymbol{\chi} \tag{2}$$

where $\mathbf{E}_s$ is the $K=M\times F$ dimensional data vector, M being the number of spatial measurement points and F the number of working frequencies, $\boldsymbol{\chi}$ is the N dimensional unknown vector, N being the number of points in D, and $\mathbf{L}$ is the $K\times N$ dimensional matrix obtained by discretizing the integral operator in eq.(1). It is worth noting that matrix $\mathbf{L}$, which state the relationship between data and unknown vectors, depends on the adopted measurement configuration. Accordingly, one needs to know the position of the measuring points to properly define $\mathbf{L}$. Herein, this information is provided by GPS as described in Section II.

The matrix inversion problem stated by eq.(2) is ill-conditioned and a regularized solution with respect to measurement uncertainties and noise is given by:

$$\tilde{\boldsymbol{\chi}}(\mathbf{r})=\sum_{n=1}^{H}\frac{\langle\mathbf{E}_s,\mathbf{u}_n\rangle}{\sigma_n}\underline{v}_n(\mathbf{r}) \tag{3}$$

In eq.(3), $\langle\cdot,\cdot\rangle$ denotes the scalar product in the data space, H is the truncation threshold, $\{\sigma_n\}_{n=1}^{K}$ is the set of singular values of the matrix $\mathbf{L}$ ordered in a decreasing way, $\{\mathbf{u}_n\}_{n=1}^{K}$

and $\{\mathbf{v}_n\}_{n=1}^{K}$ are the sets of the singular vectors. The threshold $H \leq K$ defines the "degree of regularization" of the solution and is chosen as a trade-off between accuracy and resolution requirement from one side (which should push to increase the H value) and solution stability from the other side (which should push to limit the value of H).

The imaging result is given as the spatial map of the modulus of the retrieved contrast vector $\tilde{\chi}$ normalized to its maximum value. Hence, the regions of D where the modulus of $\tilde{\chi}$ is significantly different from zero provide indication on the position and geometry of the targets.

IV. Experimental Setup

The adopted radar-equipped UAV system is shown in Figure 2. The micro UAV adopted for flight tests is a self-assembled DJI F550 hexacopter, available at the university of Naples. The F550 represents a flexible platform which can embark several auxiliary onboard systems up to a maximum payload weight close to 1 Kg.

In the configuration adopted for radar acquisition flights, it was controlled by means of a DJI Naza M-Lite autopilot (installed in the hexacopter center of mass) complemented by a remote GPS/compass installed on a mast. The autopilot enables different levels of remote control, such as manual, attitude stabilized mode, and GPS/attitude mode. The systems was flown in the last mode thus receiving commands in terms of climb rate, yaw rate, and velocity components in the horizontal directions.

The onboard payload for the radar sensing test includes the radar system, an Odroid XU4 computer running Linux operating system, a DC-DC converter, an auxiliary GPS receiver (Ublox LEA-6T) with raw data capabilities, and an associated GPS patch antenna. The radar has been installed near the battery below the center plate of the F550 frame, in order to minimize obstructions and disturbances to/from the other electronics components. Odroid, DC-DC converter, and the auxiliary GPS system, have been installed above the plate.

The Odroid XU4 has been powered by adding a custom Y connection between the F550 battery and its power distribution board. Since the battery voltage is of the order of 16 V, a lightweight DC-DC converter has been added to convert the voltage to 5 V as needed by the Odroid. The auxiliary GPS system has been powered by a USB port of the computer, which is also used for data exchange. As regards the radar, the foreseen strategy is to power it by another USB port of the Odroid computer, in order to avoid any auxiliary battery thus minimizing payload weight. This installation choice would not impact in significant way the flight autonomy, due to the very small power required by the computer (and the GPS/radar systems). However, due to output current limits of the currently available DC-DC converter, which are not compatible with the power required by the Odroid during radar transmission operation (the Odroid is itself capable of powering both GPS and radar), the first flight tests (described in this paper) were executed with an auxiliary power bank for the radar. Radar data have been exchanged via an Ethernet link and the User Datagram Protocol (UDP). The payload hardware architecture is depicted in Figure 3.

As radar we have used the on the market available PulsON 440 system [21], which is available at IREA. This is a short-range, time domain, ultra wideband system that has been chosen because it is a compact, low cost and low power platform. The sizes, indeed, are 76 mm x 80 mm x 16 mm, while the weight of the radar plus its power supply is about 200 grams. A picture of the radar is shown in Figure 3. The radar is equipped with Serial, USB and Ethernet connections and may be commanded by using a Graphical User Interface or by means of custom codes.

The radar allows monocratic measurements by using two antennas, one transmitting and the other one receiving, which are close each other. Instead of default antennas, which are shown in Figure 3, we have equipped the radar with small size log-periodic PCB antennas. In particular, Ramsey LPY26 have been used as transmitting and receiving antennas. These are directive antennas having a 6 dB gain over the frequency range from 2 GHz to 11 GHz. The antennas have been mounted in a down looking configuration (see Figure 2).

As regards data acquisition, an integrated software has been developed in C language which acquires synchronized radar and GPS data. The key implemented concepts have been to minimize latency in data acquisition and use the CPU clock to provide accurate time tagging. GPS time has been saved to enable off line analyses beyond the real time operation of the receiver. Software operation has been made easier by the fact that both radar and GPS receiver provide their data in continuous mode, once a given output frequency is selected. The radar has been programmed in such a way to acquire 10 waveforms per second, while GPS data have been acquired at 1 Hz frequency. The software has been launched remotely using the SSH tool available in Linux. A proof of accuracy in data time tagging and radar real time performance is shown in Figure 4, which reports the time interval between radar data packets (corresponding to single waveforms) as measured by the clock on the Odroid computer.

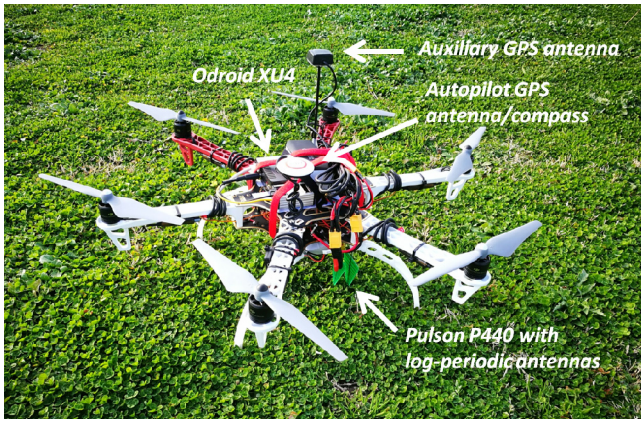

Figure 2. Hexacopter equipped with radar imaging payload

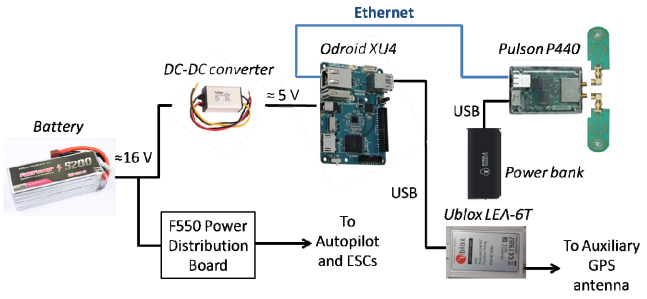

Figure 3. Payload hardware architecture

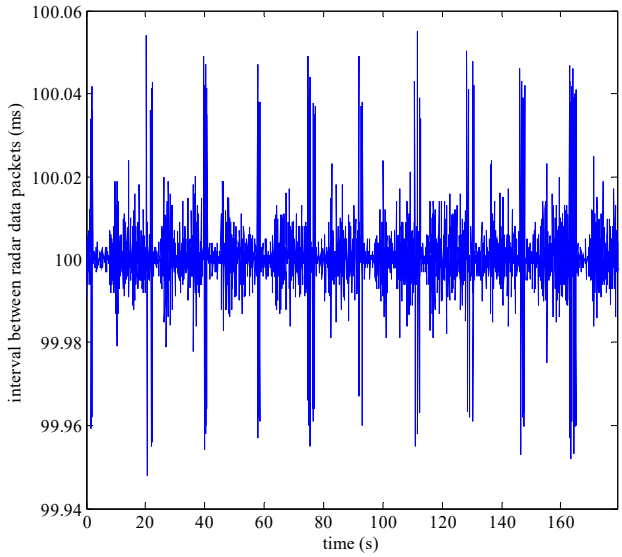

Figure 4. Time interval between subsequent radar packets, as measured by the CPU clock

V. Flight Test Results

A proof-of-concept experiment was carried out the 16th February 2017. The experiment was performed in a sunny afternoon with moderate wind conditions.

The experiment was devoted to test the ability of the assembled system to gather GPS and radar data simultaneously, and to achieve an assessment of the imaging capabilities. Therefore, metallic targets were located on the ground of the flight site. Specifically, three corner reflectors, a copper plate and an aluminum cylinder were considered. The corner reflectors were located on the ground, while the plate and the cylinder were located at 0.8 m and 0.4 m far from the air-ground interface, respectively. All the targets were aligned one to each other along a straight line.

The flight experiment lasted three minutes, during which the copter was flown above the ground targets.

The UAV path as estimated by the onboard GPS is depicted in Figure 5. It is worth noting that the reported position fix was obtained by off line processing of raw measurements and satellite ephemeris data, in order to avoid eventual latencies and errors due to position smoothing filters in the receiver firmware. It can be seen how wind disturbance affects the flight trajectory. East and North coordinates with respect to the initial position are depicted in Figure 6. Since flight was conducted in an open outdoor environment, optimal conditions were verified in terms of number of satellites in view and their geometry, as shown in Figure 7.

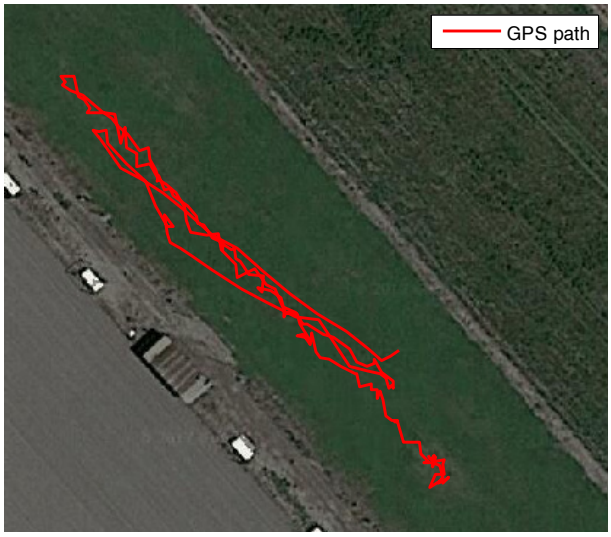

Figure 5. UAV path as estimated by GPS

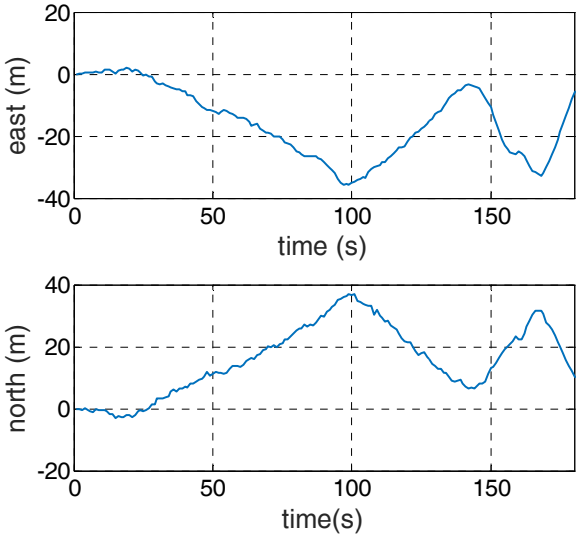

Figure 6. East and North coordinates (origin in the initial position) during flight

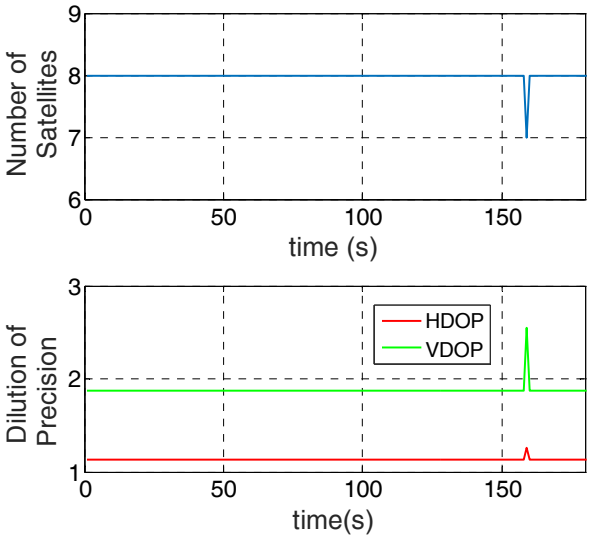

Figure 7. Number of satellites and dilution of precision during flight

As regards radar data, Figure 8 reports the overall raw data collected during the flight. Based on this figure, it is interesting to note that radar raw data enable cm-level estimation of above ground level, which can actually be exploited during processing. In fact, at each measurement time, the first peak within radar returns (corresponding to nadir) can be extracted, and then the two-way travel time of the wave can be converted into a distance measurement.

In order to test the accuracy of the target localization, more precisely the ability to obtain a focused image, we consider data gathered during a portion of the flight trajectory, which is 12.8 m long and covers the three corner reflectors, see Figure 9

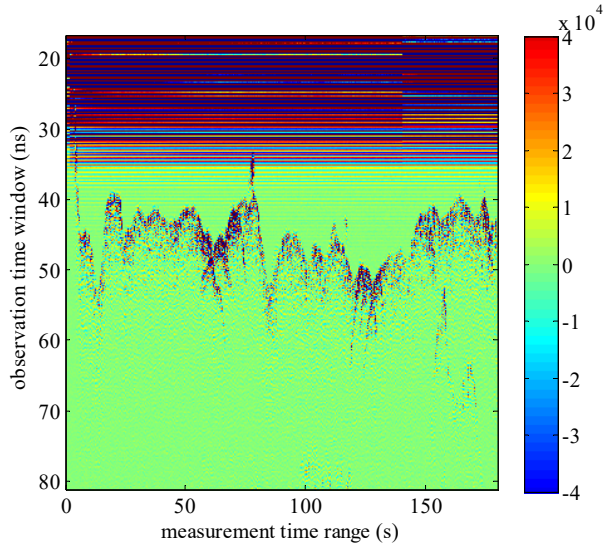

Figure 8. Overall collected radargram

Figure 9: Picture of the experimental scenario :

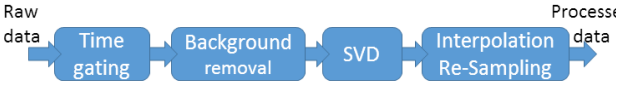

Figure 10. : Time domain data processing flow chart:

Before facing the imaging as an inverse scattering problem, as it is described in Section III, the time domain data processing approaches summarized in Figure 10have been adopted. These approaches have been used to process the back-scattered waveforms acquired into an observation time windows, which is from 16 ns to 57 ns. Figure 11a shows the considered raw radargram, wherein the corner reflectors appear as three hyperboles occurring from 49 ns up to 55 ns.

As said the raw radargram was processed according to the flow chart sketched in Figure 10.

First of all, we applied the time gating [13] in order to force to zero the portion of the radargram corresponding to antenna direct coupling and the undesired signals occurring until 40 ns .

As a second step, we adopted the background removal procedure, i.e. we subtacted from the time gated data the mean value along the *x*-direction. This procedure allows the removal of the undesired constant signals.

As a third step, we exploited a de-noising procedure, which is based on the computation of the SVD of the data matrix. In particular, let **A** be the data matrix, obtained after applying the time gating and the background removal, it is represented by means of its SVD as:

$$\mathbf{A} = \mathbf{U}\mathbf{S}\mathbf{V}^T = \sum_{i=1}^{Q} \sigma_i \mathbf{u}_i \mathbf{v}_i^T \qquad (4)$$

where **U** e **V** are orthogonal matrices having size $N \times N$ and $M \times M$, respectively; **S** is the $N \times M$ diagonal matrix whose elements are the singular values of **A** arranged in a decreasing order of magnitude and $Q \leq min\{M, N\}$ is the rank of **A** [20]. N represents the measured waveforms, M denotes the time sampling points used to represent each waveforms, and apex T denotes the transpose quantity.

The noise filtered data matrix is obtained as:

$$\tilde{\mathbf{A}} = \mathbf{A} - \sum_{i=P}^{Q} \sigma_i \mathbf{u}_i \mathbf{v}_i^T \qquad (5)$$

The threshold P is chosen as the index of the singular value in correspondence of the point where the spectrum changes its slope, i.e. the index of the singular value where the fast decay of the singular values is followed by the smooth one. According to eq. (5), we are assuming that all the singular values whose amplitude, as normalized to the maximum one, is lower than a fixed threshold are representative of the undesired portion of the measured signal. For the case at hand, the threshold P was fixed as the index of the singular value whose amplitude is 0.04 time lower than the maximum one.

As a fourth step, we performed a linear interpolation and a re-sampling of the noise filtered data. This step is necessary because the flight velocity of the UAV is not constant and thus the data samples are not spaced evenly along the measurement line. As output of this step, we obtained a data matrix made by 111 waveforms, corresponding to the backscattered signals measured at 111 measurement points evenly spaced along the 12.8 m measurement line.

Figure 11b shows the processed radargram achieved as output of the processing chain in Figure 10. The processed time domain data were used to generate the focused image appearing in Figure 11c. To obtain this latter image we computed the spectrum of the processed data into the range from 3.4 GHz to 4.6 GHz, which was sampled by using a 20 MHz step, i.e. we used 61 evenly spaced frequencies. The frequency domain data were processed by means of a linear microwave tomographic approach using the canonical 2D free space model to describe the underlying scattering phenomenon [16]. In particular, we fixed as investigation domain a rectangle, whose side was 13 m along the flight trajectory and 2 m along the range direction (i.e., the z axis). Specifically we set z_{min} = 7 m and z_{max} = 9 m.

Figure 11c corroborates that the microwave tomography approach provides a focused image from which the location and size of the targets may be inferred. In fact, the relative geometry between the first two corners is derived accurately, while a larger error is found regarding the position of the third target. It is expected that improving navigation performance can positively impact radar processing results, also allowing the selection of larger domains of investigation.

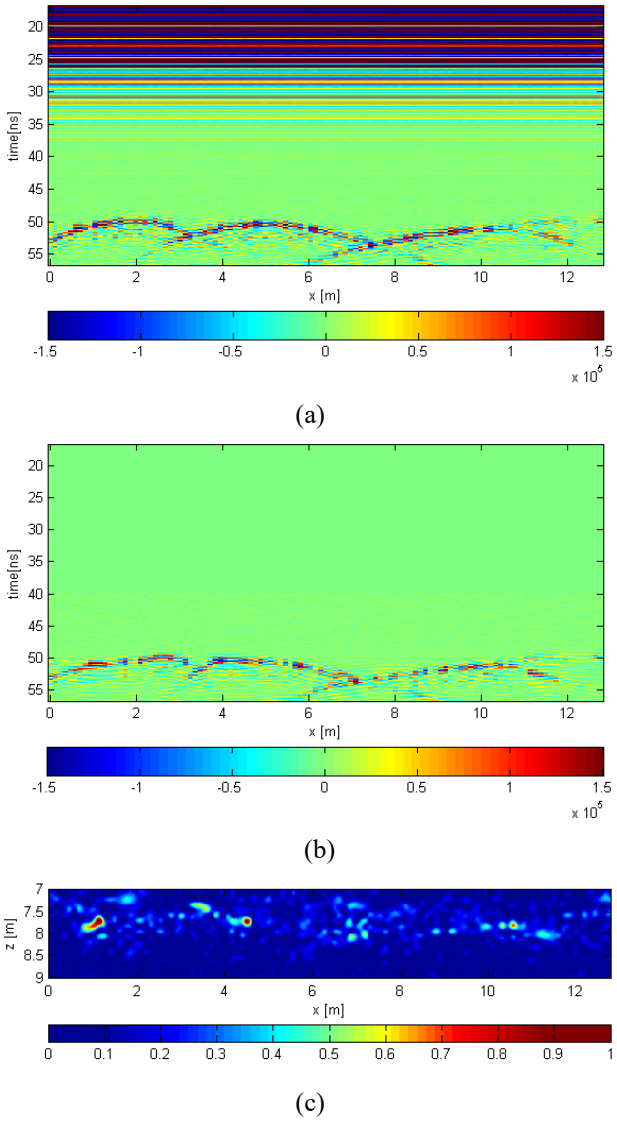

Figure 11: Result of the UAV based radar survey: a) raw radargram; b) time domain processed radargram; c) tomographic image.

VI. Conclusion

Micro-UAV-mounted radar systems are a leading edge technology for surface and subsurface imaging, and several open issues have to be addressed. Within this framework, this paper dealt with aspects related to both navigation and radar processing, and presented a radar-equipped micro-UAV system developed to support research in the field on an experimental basis.

Flight results demonstrated the capability of obtaining a focused image thus allowing accurate target localization, once navigation information is integrated within radar

imaging algorithms to compensate the effects of perturbed flight dynamics.

This encouraging preliminary result motivates to go on with the research activity, which will regard, first of all, the integration of more advanced navigation techniques. Furthermore, the capability of the considered UAV-based radar system to provide useful remote sensing information in practical missions characterized by poor visibility will be better investigated.

ACKNOWLEDGMENT

This research was carried out in the frame of Programme STAR, financially supported by UniNA and Compagnia di San Paolo, and in the framework of "Programma per il finanziamento della ricerca di Ateneo" funded by UniNA. The authors thank Dr. Roberto Opromolla for support during experimental tests.

REFERENCES

[1] D. Floreano and R. J. Wood, Science, technology and the future of small autonomous drones, Nature 2015, doi:10.1038/nature14542.

[2] K. Whitehead, C. H. Hugenholtz, "Remote sensing of the environment with small unmanned aircraft systems (UASs), part 1: a review of progress and challenges", J. Unmanned Vehicle Systems, vol.2, pp. 69-85, 2014

[3] F. Nex and F. Remondino, UAV for 3D mapping applications: a review, Applied Geomatics, vol.6(1), pp.1-15, 2014

[4] I. Catapano et al., A tomographic approach for helicopter-borne ground penetrating radar imaging IEEE Geosci. and Remote Sens. Lett.,vol. 9 (3), pp. 378-382. 2012.

[5] K. Ouchi, Recent trend and advance of synthetic aperture radar with selected topics, Remote Sens, vol.5, pp.716-807, 2013.

[6] D. Altdor et al., UAV-borne electromagnetic induction and ground-penetrating radar measurements: a feasibility test, 74th Annual Meeting of the Deutsche Geophysikalische Gesellschaft in Karlsruhe, Germany, March 9 - 13, 2014.

[7] A. F. Scannapieco, A. Renga, G. Fasano, A. Moccia, Ultralight radar sensor for autonomous operations by micro-UAS, International Conference on Unmanned Aircraft Systems (ICUAS), Arlington, VA, USA, June 2016, pp. 727-735

[8] R. J. Cosentino, D. W. Diggle, M. U. de Haag, C. J. Hegarty, D. Milbert, and J. Nagle, "Differential GPS," in Understanding GPS—Principles and Applications, E. D. Kaplan and C. J. Hegarty, Eds., Artech House, London, UK, 2nd edition, 2006.

[9] J. Liu, M. E. Cannon, P. Alves, M. G. Petovello, G. Lachapelle, G. MacGougan, and L. deGroot, "A performance comparison of single and dual frequency GPS ambiguity resolution strategies," GPS Solut., vol. 7, no. 2, pp. 87–100, 2003.

[10] GPS SPS Performance Standard (4th edition, September 2008)

[11] R. Conley, R. J. Cosentino, C.J. Hegarty, E. D. Kaplan, J. L. Leva, M. U. de Haag, K. Van Dyke, Performance of Stand-Alone GPS, in in Kaplan, E.D., Hegarty, C. J.,Understanding GPS – Principles and Applications, 2nd Edition, Artech House, Boston/London, 2006.

[12] L. Serrano, D. Kim, R. B. Langley, A GPS Velocity Sensor: How Accurate Can It Be? – A First Look, ION NTM 2004, 26-28 January 2004, San Diego, CA, 875-885.

[13] D. J. Daniels, Ed., Ground Penetrating Radar. The Institution of Electrical Engineers (IEE), London, UK, 2nd ed., 2004.

[14] I. Catapano, A. Randazzo, E. Slob, R. Solimene, "GPR imaging via qualitative and quantitative approaches", Civil Engineering Applications of Ground Penetrating Radar, pp. 239-280, Springer International Publishing, 2015

[15] F. Soldovieri, J. Hugenschmidt, R. Persico, G. Leone, A linear inverse scattering algorithm for realistic GPR applications, Near Surface Geophysics, vol.5(1), pp.29-41, Feb. 2007

[16] I. Catapano, F. Soldovieri, M.A. González-Huici, Performance assessment of a microwave tomographic approach for the Forward Looking Radar configuration, Sens. Imaging, vol.91(1), 13pp, Apr. 2014.

[17] I. Catapano, L, Crocco, Y. Krellmann, G. Triltzsch, F. Soldovieri, Tomographic airborne ground penetrating radar imaging: Achievable spatial resolution and on-field assessment, ISPRS J. of Photogrammetry and Remote Sens., vol.92, pp.69-78, June 2014.

[18] I. Catapano, A. Affinito, G. Gennarelli, F. di Maio, A. Loperte, F. Soldovieri, Full three-dimensional imaging via ground penetrating radar: assessment in controlled conditions and on field for archaeological prospecting, Applied Physics A, vol. 115(4), pp.1415-1422, June 2014.

[19] W.C. Chew, Waves and Fields in Inhomogeneous Media, 2nd ed. New York: IEEE, 1995

[20] M. Bertero and P. Boccacci, Introduction to Inverse Problems in Imaging, Inst. Physics Publ., London, UK, 1998

[21] http://www.timedomain.com/products/pulson-440/.